NANO LETTERS

pubs.acs.org/NanoLett

Letter

Experimental Observation of Flat Bands in One-Dimensional Chiral Magnonic Crystals

Silvia Tacchi,* Jorge Flores-Farías, Daniela Petti,* Felipe Brevis, Andrea Cattoni, Giuseppe Scaramuzzi, Davide Girardi, David Cortés-Ortuño, Rodolfo A. Gallardo, Edoardo Albisetti, Giovanni Carlotti, and Pedro Landeros*

Cite This: *Nano Lett.* 2023, 23, 6776−6783

Read Online

ACCESS | Metrics & More | Article Recommendations | Supporting Information

ABSTRACT: Spin waves represent the collective excitations of the magnetization field within a magnetic material, providing dispersion curves that can be manipulated by material design and external stimuli. Bulk and surface spin waves can be excited in a thin film with positive or negative group velocities and, by incorporating a symmetry-breaking mechanism, magnetochiral features arise. Here we study the band diagram of a chiral magnonic crystal consisting of a ferromagnetic film incorporating a periodic Dzyaloshinskii−Moriya coupling via interfacial contact with an array of heavy-metal nanowires. We provide experimental evidence for a strong asymmetry of the spin wave amplitude induced by the modulated interfacial Dzyaloshinskii−Moriya interaction, which generates a nonreciprocal propagation. Moreover, we observe the formation of flat spin-wave bands at low frequencies in the band diagram. Calculations reveal that depending on the perpendicular anisotropy, the spin-wave localization associated with the flat modes occurs in the zones with or without Dzyaloshinskii−Moriya interaction.

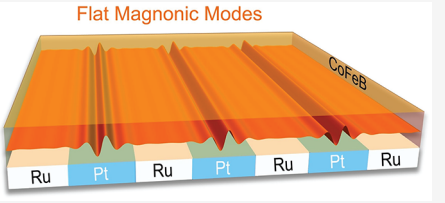

KEYWORDS: *flat bands, chiral magnonic crystals, spin waves, Dzyaloshinskii−Moriya, thin films, Brillouin light scattering*

In the past decade, the research field of magnonics has rapidly grown due to its potential for the development of innovative low-energy computing devices, where spin waves (SWs), the collective excitations of electron spins, are used to carry and process information.[1−3] Progress in this field mainly relies on the capability to control and manipulate the SW propagation, for the implementation of SW-based devices with unprecedented functionalities in information and communication technologies.[4−7] In this context, the exploitation of the interfacial Dzyaloshinskii−Moriya interaction (i-DMI),[8−10] namely the antisymmetric exchange interaction arising at the interface of a ferromagnetic film and a heavy-metal substrate with high spin−orbit coupling,[11−14] can represent an effective method for achieving a nonreciprocal SW propagation, opening the way toward unidirectional devices such as insulators and diodes for nanomagnonic circuits.[15−19] The nonreciprocal magnonic propagation, induced by the presence of i-DMI, has been primarily used to quantify the i-DMI strength, D, in continuous metallic films and multilayers.[20−26] In this respect, a small i-DMI has also been observed in magnetic garnet systems in contact with heavy metals,[27−30] which are auspicious materials for magnonic applications due to their low damping. Nevertheless, typical values of the i-DMI strength are still 2 orders of magnitude smaller than for conventional ferromagnets.[31,32] A frequency nonreciprocity can also originate from any symmetry-breaking mechanism along the thickness, such as different anisotropies at the bottom and top surfaces,[33] magnetization grading,[34] and dipolar coupling in bilayers[35−37] and curved surfaces.[38,39] However, such effects are negligible in ultrathin films.

More recently, i-DMI has been theoretically proposed as an additional means to tailor the band diagram of chiral magnonic crystals (MCs), artificial structures where a periodic modulation of the magnetic properties is used to control SW propagation.[40−43] In magnetic nanostructures, the nonreciprocity caused by the i-DMI together with the confined geometry leads to a fixed nodal structure with amplitudes modulated in time and a phase velocity defined by the differences among opposing waves.[44] Micromagnetic simulations[40] and calculations[41] on a surface-modulated magnonic crystal incorporating a continuous i-DMI show the features of both a conventional MC and a nonreciprocal system, namely bandgaps with indirect gaps. For a slightly different system, consisting of a one-dimensional MC formed by a continuous magnetic film in contact with a regular array of heavy-metal stripes, calculations predicted that the periodic modulation of the i-DMI induces the appearance of flat magnonic modes localized underneath the heavy-metal stripes.[43] These bands

Received: October 27, 2022
Revised: May 30, 2023
Published: June 21, 2023

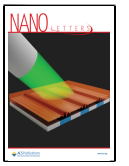

https://doi.org/10.1021/acs.nanolett.2c04215
Nano Lett. 2023, 23, 6776−6783

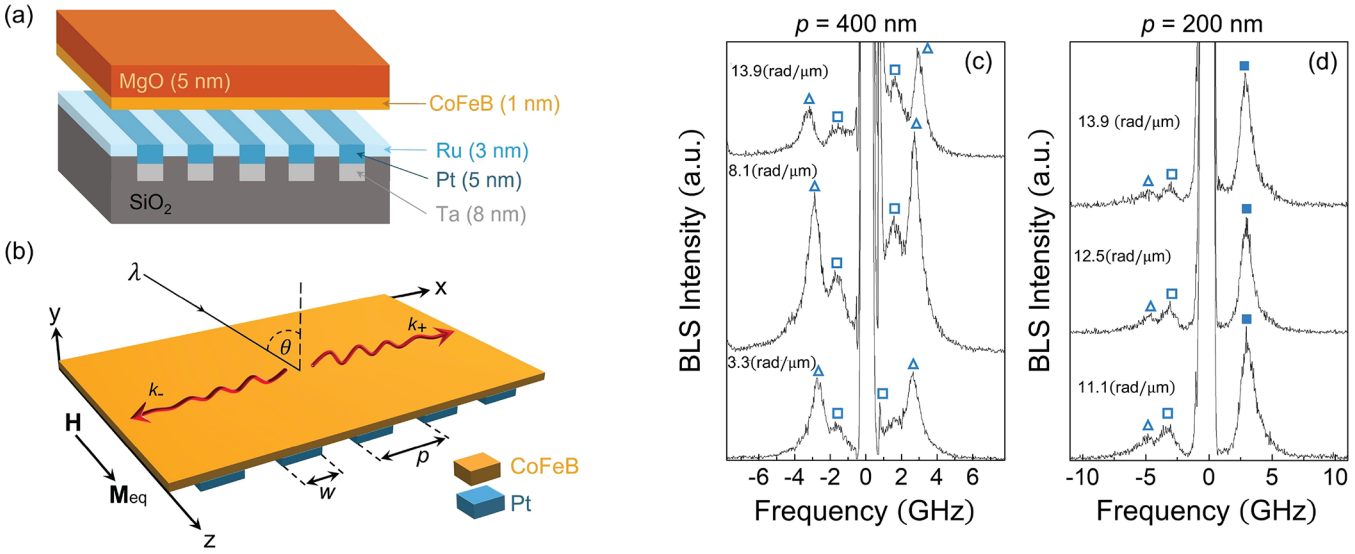

Figure 1. (a) Schematic picture of the investigated chiral magnonic crystal. The system consists of a periodic array that alternates platinum and ruthenium nanostripes of width w and period p capped with a 1 nm CoFeB film. (b) Spin waves propagating in the Damon−Eshbach configuration along the x axis, while the applied field and equilibrium magnetization point along the z axis. Brillouin spectra measured for the samples having Pt stripe periods (c) p = 400 nm (and stripe width w = 200 nm) and (d) p = 200 nm (and w = 160 nm), at different values of the in-plane transferred wave vector indicated in every spectrum, for a magnetic field $\mu_0 H$ = 50 mT applied along the stripe axis. Triangles and squares indicate the different modes. In (d), the full squares identify the peaks with large intensities, and a noticeable difference between the anti-Stokes (right) and Stokes (left) sides of the spectra is observed.

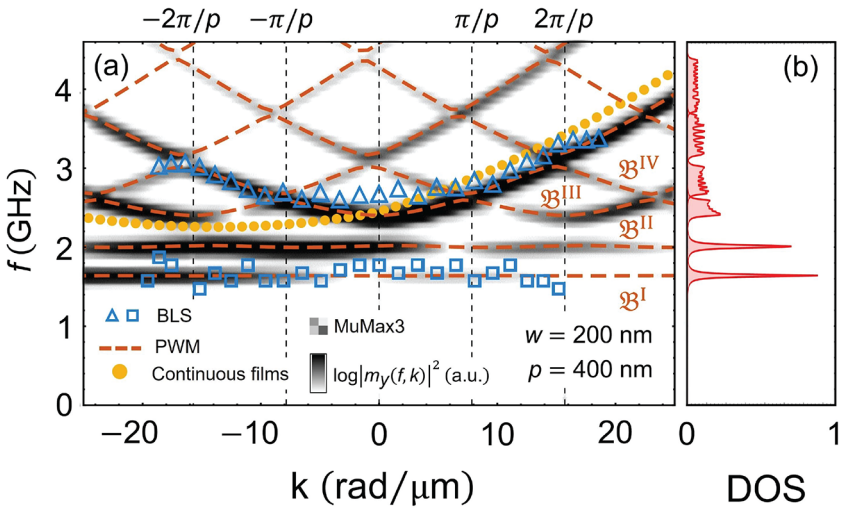

Figure 2. (a) Magnonic band structure of the chiral magnonic crystals with period p = 400 nm and Pt wire width w = 200 nm. The open symbols represent the BLS data, the dashed lines indicate the PWM calculations, and the gray color represents the power spectrum of the out-of-plane component of the dynamic magnetization obtained from MuMax3 simulations, with the strength indicated by the color bar. The full orange circles depict the dispersion calculated for a continuous film having an effective and homogeneous i-DMI distributed over the entire film. (b) Calculated density of states (DOS) of the same sample, where the sharp peaks at low frequency are the fingerprints of the flat bands.

are separated by indirect frequency gaps, whose amplitude depends on both the i-DMI strength and the geometry associated with the artificial periodicity. Moreover, dispersionless flat bands and a robust nonreciprocal character of the band diagram are observed for relatively large values of the i-DMI, above a threshold value that depends on the sample and periodicity of the array (see Figure 2g in ref 43). In this respect, it is worth noting that the design and realization of metamaterials with tailored band structures, that permit quasiparticle control, are of great interest not only in magnonics but also in the research fields of photonics, electronics, plasmonics, and phononics.[45−48] The formation of flat bands[49,50] is a particularly interesting behavior, because when the group velocity is notably reduced, and the associated quasiparticle loses its kinetic energy, strongly interacting phases of matter can develop.[51−54] Flat bands have been recently reported in nonmagnetic systems[55−58] and in different forms of magnetic metamaterials without i-DMI, such as 1D MCs[59−63] and 2D MCs,[64] consisting of both dot and antidot arrays. Flat bands have also been reported in ferromagnetic and antiferromagnetic crystal lattices.[65−69] Nonetheless, the appearance of flat modes and, more generally, a detailed analysis of the influence of the periodic i-DMI on the

https://doi.org/10.1021/acs.nanolett.2c04215
Nano Lett. 2023, 23, 6776−6783

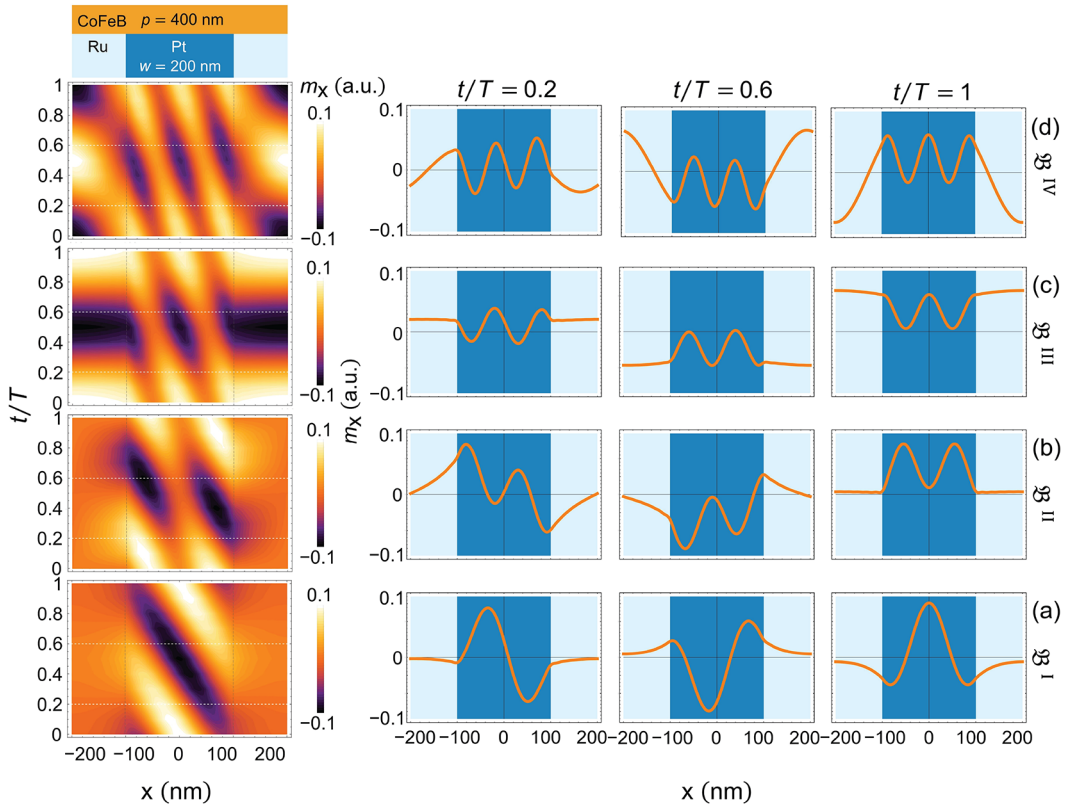

Figure 3. Spatiotemporal profiles of the dynamic magnetization component m_x in a unit cell for $k = \pi/p$ and for the first four low-frequency bands: (a) $\mathcal{B}^{I}$, (b) $\mathcal{B}^{II}$, (c) $\mathcal{B}^{III}$, and (d) $\mathcal{B}^{IV}$. The blue (light blue) color illustrates the zones with (without) i-DMI. In the right panels, three times are considered, which are highlighted with the dashed horizontal lines, where T is the period of the oscillation.

magnonic band structure of MCs have not been experimentally proved up to now.

In this work we perform a combined theoretical and experimental investigation of the influence of a periodic i-DMI on the magnonic band diagram of one-dimensional chiral magnonic crystals, consisting of a 1 nm thick CoFeB film deposited on top of a regular array of heavy-metal nanostrips. Using Brillouin light scattering (BLS), we experimentally demonstrate that the presence of a periodic i-DMI produces localized flat modes and asymmetric SW propagation. A strong nonreciprocal character of the BLS intensity is further observed, which practically suppresses SW propagation of the second mode for one wave-vector direction. Calculations and micromagnetic simulations support the experimental observations and shed light on the observed nonreciprocity and on the spatial localization of the detected modes.

The investigated samples consist of extended CoFeB films of 1 nm thickness sitting over an array of Pt nanostripes with a thickness of 5 nm. The Pt stripes alternate with Ru stripes and are embedded in a SiO_2 substrate, as shown in Figure 1a. Atomic force microscopy (AFM) reveals that the Pt/Ru surface presents a modulation of the thickness with small steps ranging from 0.5 to 4 nm due to the fabrication process, as depicted in Figures S1 and S2 of the Supporting Information. As the deposition of the CoFeB is performed by magnetron sputtering, the magnetic layer morphology is conformal with the Pt/Ru surface. BLS measurements have been performed applying an external magnetic field $\mu_0 H = 50$ mT (Figure 1b) along the stripes, which is strong enough to saturate the magnetization, as revealed by magnetic force microscopy measurements (not shown). BLS spectra measured for the samples having a Pt stripe period $p = 400$ nm (with stripe width $w = 200$ nm) and $p = 200$ nm (with stripe width $w = 160$ nm) are shown in Figure 1c,d, respectively. For the sample having a stripe period $p = 400$ nm, two modes are detected in both the Stokes ($f < 0$) and the anti-Stokes ($f > 0$) sides of the BLS spectra. As can be seen, the peak at a higher frequency has a stronger BLS intensity, and its frequency increases with the wave vector. In addition, this mode is characterized by a slight frequency asymmetry between the Stokes and the anti-Stokes sides, which reverses on reversing the external field direction. See Figure S3 in the Supporting Information. On the contrary, a dispersionless behavior characterizes the peak at a lower frequency. Note that, although in the Damon−Eshbach geometry different interface anisotropies at the top and bottom surfaces of a magnetic film might lead to a small nonreciprocity of the SW frequency, in our sample this effect is negligible due to the ultrathin thickness of the CoFeB film,[33,70] so that the frequency asymmetry can be totally ascribed to the i-DMI. For the samples having smaller periodicity (Figure 1d), the BLS data are characterized by a marked qualitative change, featuring a strong nonreciprocal BLS intensity. In particular, two peaks, having similar intensity, are visible on the Stokes side, while only the lowest frequency peak, having a considerable intensity, is present on the anti-Stokes side. Furthermore, both peaks show an almost constant frequency as a function of the wave vector, indicating the flattening of the low-frequency band.

The measured magnonic band structure for the sample with stripe period $p = 400$ nm are displayed in Figure 2a by the blue symbols (open squares for the lowest band and open triangles for the upper band). The dashed lines correspond to the plane-wave method (PWM) calculations,[82] where $\mathcal{B}^n$ represents the

https://doi.org/10.1021/acs.nanolett.2c04215
Nano Lett. 2023, 23, 6776−6783

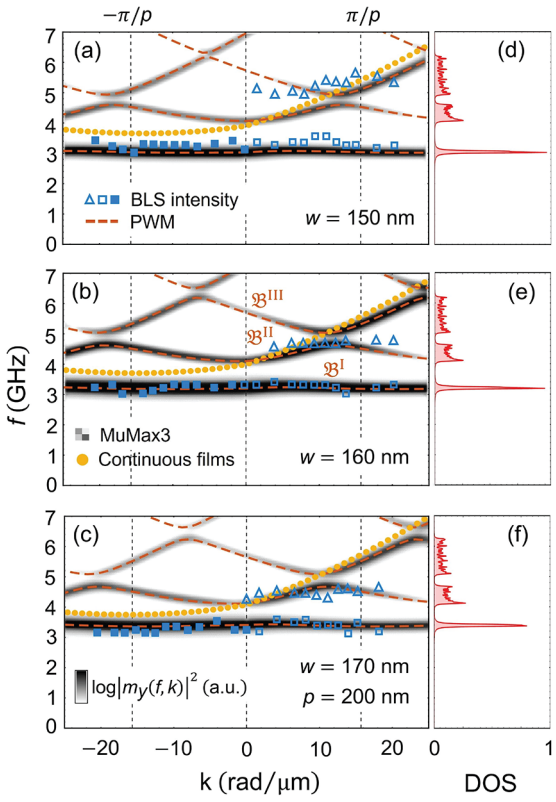

Figure 4. Band structure for the chiral magnonic crystals with p = 200 nm and three widths of the platinum wires: (a) w = 150 nm, (b) w = 160 nm, and (c) w = 170 nm. The symbols correspond to the BLS data and the dashed lines to the PWM calculations, and the gray color map represents the power spectrum of the out-of-plane component of the dynamic magnetization obtained from MuMax3 simulations with the strength indicated by the color bar. To emphasize the BLS intensities of the Stokes and anti-Stokes sides of the experimental spectra, filled square markers have been considered to identify the peaks with the largest BLS intensities. The full orange circles depict the dispersion calculated for a continuous film having effective and homogeneous i-DMI distributed over the entire film. (d−f) Calculated magnonic density of states, where a large sharp peak is a fingerprint of a flat band.

nth band, and n = I, II, III, IV is the band index. The gray color map in the background represents the power spectrum of the out-of-plane component of the dynamical magnetization obtained by the micromagnetic simulations, while the full orange circles depict the dispersion calculated for a continuous film with an effective i-DMI constant $D_{\mathrm{eff}} = (w/p)D$, which represents the averaged DM constant distributed over the entire film. As the AFM measurements reveal, the growth process induced a tiny stripe-like geometrical modulation of 0.5−4 nm, which could modify the band structure.[82] Nevertheless, in our geometry, where the magnetization is parallel to the stripe axis, no significant influence in the spin-wave dispersion is expected,[71,72] because only dynamic magnetic charges are induced at the stripe edges, which are not strong enough to alter the magnonic band structure significantly.[62,73,74] A good agreement with the frequency and wave vectors of the BLS data has been found by setting slightly different values of the effective magnetization due to the different perpendicular magnetic anisotropy at the Pt and the Ru interface.[75] Specifically, for the regions in contact with Pt, $\mu_0 M_{\mathrm{eff}}^{(\mathrm{Pt})}$ = 95.8 mT, and for the case of Ru, $\mu_0 M_{\mathrm{eff}}^{(\mathrm{Ru})}$ = 75.8 mT, for an exchange constant A_{ex} = 15.62 pJ/m and an i-DMI strength D = 1.1 mJ/m^2 in the Pt zones. In particular, the lower value of M_{eff} in the region in contact with Ru can be ascribed not only to the perpendicular magnetic anisotropy but also to a reduction of the saturation magnetization due to the interdiffusion and dead layer formation at the Ru/CoFeB interface.[75−77] The positive value of M_{eff} indicates a remanent state with in-plane magnetization, as found experimentally.

The data for the low-frequency band in Figure 2a show a magnonic dispersion nearly independent of the momentum, in agreement with recent theoretical predictions.[43] Note that the flattening of the low-frequency magnonic bands directly affects the SW propagation since the transport of energy is related to the group velocity $v_g = 2\pi\nabla_k f$. In order to highlight the flattening of the low-frequency bands, we have calculated the density of states (DOS)[78] in Figure 2b, where large sharp peaks identify flat bands because the DOS is inversely proportional to v_g. In this case, there are two sharp peaks around 1.6 and 2 GHz, where the low-frequency flat band $\mathcal{B}^{\mathrm{I}}$ shows the largest peak. When the dispersion slope tends to zero, there is no energy transport, and the SWs localize in specific regions of the chiral MC, depending on the band. For the first band, a group velocity of less than 0.01 km/s is estimated along the propagation direction x, which shows a notable reduction with respect to the large group velocity in a thin film with a continuous i-DMI (about 0.8 km/s). By analyzing the perfect-film dispersion with $D_{\mathrm{eff}} = (w/p)D$, which represents the film-averaged DMI constant (full orange dots), one can observe that the inclusion of periodic i-DMI changes the dynamic response of the film, by distributing the energy of the perfect-film's mode between the SW modes of the magnonic crystal. In other words, a significant power-spectrum amplitude is expected for frequencies close to the perfect-film dispersion, leading to a higher intensity of the first band for negative k. We also observe a difference in the MuMax3 power-spectrum amplitude of counter-propagating SWs. This behavior is also evidenced in the amplitude asymmetry between the measured Stokes and anti-Stokes peaks, although other complex factors (such as magneto-optical coefficients, light polarization, spin−spin correlation function, etc.) may contribute to the BLS intensity asymmetry.[79−81] These factors, which are not considered in the simulations, are included in the BLS cross-section. A quantitative comparison of the simulated power spectrum and the BLS intensities is beyond the scope of this work.

The localization of the magnons can be seen in the calculated spatial profiles of the dynamic magnetization (Figure 3). The spatiotemporal evolution of the first four bands is illustrated for $k = \pi/p$, evidencing a fairly different behavior in the zones with and without i-DMI. It is observed that the first two bands, $\mathcal{B}^{\mathrm{I}}$ and $\mathcal{B}^{\mathrm{II}}$, localize in the region that is in contact with Pt, where the i-DMI is active, with an almost zero dynamic component in the regions without Pt. This indicates that the formation of the flat bands can be ascribed to the notable reduction of the internal field in the zones with i-DMI, localizing the low-frequency excitations at these regions and forming standing waves or flat bands with nearly zero group velocity.

In order to study the influence of the periodicity on the band structure, three samples with a lower value of the lattice parameter were analyzed. The measured magnonic dispersions for three samples with stripe period p = 200 nm and widths (a)

https://doi.org/10.1021/acs.nanolett.2c04215
Nano Lett. 2023, 23, 6776−6783

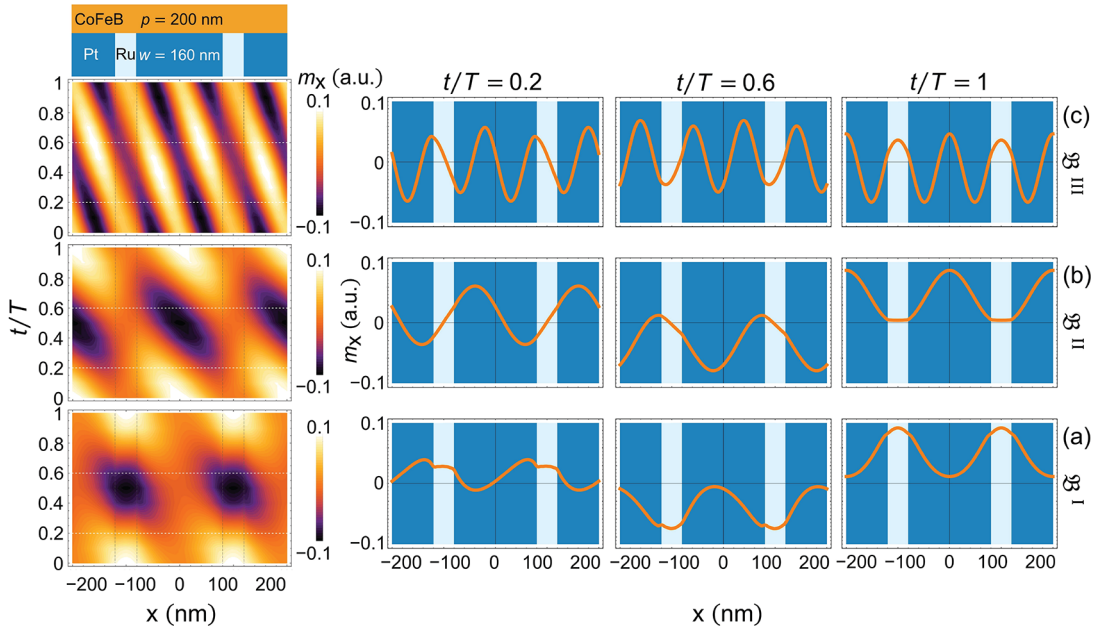

Figure 5. Spatiotemporal profiles of the dynamic magnetization component m_x evaluated for $k = \pi/p$, and for the first three bands of the sample with w = 160 nm: (a) $\mathcal{B}^{I}$, (b) $\mathcal{B}^{II}$, and (c) $\mathcal{B}^{III}$. The blue (light blue) color illustrates the zones with (without) interfacial DMI. In the right panels, three times are considered, which are highlighted with the dashed horizontal lines, where T is the period of the oscillation.

w = 150 nm, (b) w = 160 nm, and (c) w = 170 nm are displayed in Figure 4 by the blue symbols. As in the previous figure, the orange dashed lines correspond to the PWM calculations, the gray code represents the power spectrum of the out-of-plane component of the dynamical magnetization simulated by MuMax3, and the full orange circles depict the dispersion of a continuous film with an effective DMI constant D_{eff}. Calculations and simulations agree with the BLS measurements, where the theory used $\mu_0 M_{eff}^{(Pt)} = 375.8$ mT in the Pt region and $\mu_0 M_{eff}^{(Ru)} = 55.8$ mT in the Ru region. The relatively larger value of $\mu_0 M_{eff}$ in the Pt region may reflect either a decrease of the perpendicular anisotropy field with respect to the previous sample (p = 400 nm) or a moderate increase of the saturation magnetization in these samples. Figure 4d–f shows the calculated density of states (DOS),[78] where a strong peak identifies a flat band.

Compared to the previous sample (with p = 400 nm), the BLS data for p = 200 nm show a stronger asymmetry in the amplitude of the SW modes (see Figure 1d). This behavior cannot be explained with the PWM theory nor the MuMax3 simulations since the BLS intensity depends on additional factors, as explained before. However, the analysis of the dispersion of the continuous film may help to understand the asymmetry in the BLS intensities qualitatively. In Figures 2 and 4, it is observed that the measured modes close to the film dispersion exhibit a higher BLS intensity. Hence, despite the complexity of the samples, this kind of magnonic crystal can be seen as an effective continuous film perturbed with the periodic potential produced by the Pt stripes. On the other hand, one can also observe that the number of flat bands depends on the period p. In Figure 2, we see two flat bands, while only a single flat band appears for the smaller period (Figure 4). This behavior is due to the modification of the Brillouin zone (BZ), which is inversely proportional to p. Then, for a larger period (p = 400 nm), the BZ is reduced, and the bands are less dispersive within this zone, enhancing the flattening of the bands. In contrast, the BZ increases for a small periodicity (p = 200 nm), and the SWs are excited at large wave vectors, where the dispersive character of the waves increases due to the exchange interaction, inhibiting the formation of the flat bands.

As an illustration, for samples with p = 200 nm and w = 160 nm, Figure 5 shows the temporal evolution of the in-plane dynamic magnetization component, m_x, for the three first modes evaluated at $k = \pi/p$. As can be seen in Figure 5a, the magnetization oscillations of the low-frequency mode, $\mathcal{B}^{I}$, are given mainly in the Ru zone without i-DMI, even when the zone with Pt is relatively large compared to it. This unexpected dynamic behavior is associated with the noticeable difference in the effective magnetization mentioned above, so that the magnetic moments are more likely to be localized in the low-frequency state in the Ru zone where a weaker effective magnetization is present. Conversely, the second mode is localized in the zones with i-DMI, while the third mode has a propagative nature, with an almost delocalized character. This last feature is reflected in the appreciable slope of the related dispersion curves, which are largely superimposed with that of the extended film with continuous i-DMI (full orange dots in Figure 4b). It is worth mentioning that the almost flat bands reported here have been achieved for a relatively modest value of the i-DMI strength (about 1.1 mJ/m^2), compared to experimentally reported values.[31,32] As the Dzyaloshinskii–Moriya constant increases, the frequency of the SWs is reduced for one SW direction. Therefore, it is expected that the magnetization amplitude should be more pronounced in the zones with Pt, because for larger i-DMI values the frequency minimum is lower in the Pt zones (not shown). For such slightly larger values of D, around 2 or 3 mJ/m^2, the band flattening increases noticeably,[43] improving the magnon localization in the zones with periodic i-DMI.

Comparing the samples with p = 200 nm and p = 400 nm, one can observe that micromagnetic simulations show a different tendency in the power-spectrum amplitude in the two

https://doi.org/10.1021/acs.nanolett.2c04215
Nano Lett. 2023, 23, 6776–6783

nanostructures. On the one hand, the case p = 400 nm depicts two flat bands with a notorious nonreciprocity in the simulated amplitude, being more prominent in the negative wave-vector range. On the other hand, the sample with a lattice parameter p = 200 nm shows an almost reciprocal power-spectrum amplitude. This behavior of the simulated power spectrum is attributed to the different nature of the SW localization in the samples. As observed in Figure 3, for the case p = 400 nm, the first two low-frequency bands are mostly excited in the Pt zones, where the i-DMI is present. Thus, such flat bands are nonreciprocal in amplitude due to the chiral nature of the Dzyaloshinskii–Moriya interaction. In contrast, in the sample with p = 200 nm, the low-frequency flat mode is located underneath the Ru regions (see Figure 5), where the amplitude of these modes tends to be reciprocal. Overall, by tuning system parameters such as the effective magnetization and DMI constant, it is possible to manipulate the character of the SW localization and, therefore, the asymmetric amplitude effect.

In conclusion, we have investigated the influence of a periodic i-DMI on the magnonic band diagram of one-dimensional chiral MCs, consisting of an ultrathin ferromagnetic film deposited on top of a regular array of heavy-metal stripes. We experimentally demonstrate that the modulation of the i-DMI causes a strong asymmetry of the SW amplitude, suppressing SW propagation for one wave-vector direction. Moreover, the formation of flat SW bands at low frequency is observed in the band diagram. Theoretical calculations show that the spatial profiles of the flat modes exhibit a notable localization in the zones with or without i-DMI, depending on the perpendicular anisotropy, which varies with the material (Pt or Ru) in contact with the magnetic film. Our findings pave the way for the design and realization of metamaterials with tailored band structures that permit quasiparticle control and are, hence, of great interest for prospective magnonic applications.

■ ASSOCIATED CONTENT

Supporting Information

The Supporting Information includes The Supporting Information is available free of charge at https://pubs.acs.org/doi/10.1021/acs.nanolett.2c04215.

Details of the sample fabrication, BLS measurements, and theoretical methods, such as the plane-wave method and micromagnetic simulations, and further information about the dependence of the magnon bands on the sample period and the physical origin behind the formation of flat magnonic bands (PDF).

■ AUTHOR INFORMATION

Corresponding Authors

Silvia Tacchi − *Istituto Officina dei Materiali del CNR (CNR-IOM), Sede Secondaria di Perugia, c/o Dipartimento di Fisica e Geologia, Università di Perugia, 06123 Perugia, Italy*; Email: tacchi@iom.cnr.it

Daniela Petti − *Dipartimento di Fisica, Politecnico di Milano, Milano 20133, Italy*; Email: daniela.petti@polimi.it

Pedro Landeros − *Departamento de Física, Universidad Técnica Federico Santa María, Valparaíso 2390123, Chile*; orcid.org/0000-0002-0927-1419; Email: pedro.landeros@usm.cl

Authors

Jorge Flores-Farías − *Departamento de Física, Universidad Técnica Federico Santa María, Valparaíso 2390123, Chile*; orcid.org/0009-0009-4295-6098

Felipe Brevis − *Departamento de Física, Universidad Técnica Federico Santa María, Valparaíso 2390123, Chile*; orcid.org/0000-0001-8535-3187

Andrea Cattoni − *Centre de Nanosciences et de Nanotechnologies (C2N), CNRS, Université Paris-Saclay, Palaiseau 91120, France*; orcid.org/0000-0002-6402-0911

Giuseppe Scaramuzzi − *Dipartimento di Fisica, Politecnico di Milano, Milano 20133, Italy*

Davide Girardi − *Dipartimento di Fisica, Politecnico di Milano, Milano 20133, Italy*

David Cortés-Ortuño − *Departamento de Física, Universidad Técnica Federico Santa María, Valparaíso 2390123, Chile*

Rodolfo A. Gallardo − *Departamento de Física, Universidad Técnica Federico Santa María, Valparaíso 2390123, Chile*

Edoardo Albisetti − *Dipartimento di Fisica, Politecnico di Milano, Milano 20133, Italy*; orcid.org/0000-0002-8134-0482

Giovanni Carlotti − *Dipartimento di Fisica e Geologia, Università di Perugia, 06123 Perugia, Italy*

Complete contact information is available at: https://pubs.acs.org/10.1021/acs.nanolett.2c04215

Notes

The authors declare no competing financial interest.

■ ACKNOWLEDGMENTS

Financial support from the following sources is kindly acknowledged: Fondecyt, Grants 1201153 and 1210607, Basal Program for Centers of Excellence, Grant AFB220001 CEDENNA (Chile), Italian national project IT-SPIN (PRIN-2020LWPKH7), and NextGenerationEU National Innovation Ecosystem grant ECS00000041−VITALITY, under the Italian Ministry of University and Research (MUR). D.C.-O. acknowledges support by the DGIIE (UTFSM) through the Postdoctoral initiative, and F.B. aknowledges support form ANID Ph.D. grant 2021-21211469. This paper is part of a project that has received funding from the European Union's Horizon 2020 research and innovation program under Grant Agreement Number 948225, Project B3YOND. This work has been supported by the FARE programme of the Italian Ministry for University and Research (MUR) under grant agreement R20FC3PX8R (project NAMASTE). This work has been supported by Fondazione Cariplo and Fondazione CDP, grant no. 2022-1881. The work was partly supported by the French Renatech network. This work was partially performed at Polifab, the micro- and nanotechnology center of the Politecnico di Milano.

■ REFERENCES

(1) Krawczyk, M.; Grundler, D. Review and prospects of magnonic crystals and devices with reprogrammable band structure. *J. Phys.: Condens. Matter* **2014**, *26*, 123202.

(2) Chumak, A. V.; Vasyuchka, V. I.; Serga, A. A.; Hillebrands, B. Magnon spintronics. *Nat. Phys.* **2015**, *11*, 453−461.

(3) Barman, A.; et al. The 2021 Magnonics Roadmap. *J. Phys.: Condens. Matter* **2021**, *33*, 413001.

(4) Pirro, P.; Vasyuchka, V. I.; Serga, A. A.; Hillebrands, B. Advances in coherent magnonics. *Nat. Rev. Mater.* **2021**, *6*, 1114−1135.

(5) Chen, J.; et al. Reconfigurable Spin-Wave Interferometer at the Nanoscale. *Nano Lett.* **2021**, *21*, 6237−6244.
(6) Chumak, A. V.; et al. Advances in Magnetics Roadmap on Spin-Wave Computing. *IEEE Trans. Magn.* **2022**, *58*, 1−72.
(7) Petti, D.; Tacchi, S.; Albisetti, E. Review on magnonics with engineered spin textures. *J. Phys. D: Appl. Phys.* **2022**, *55*, 293003.
(8) Dzyaloshinsky, I. A thermodynamic theory of "weak" ferromagnetism of antiferromagnetics. *J. Phys. Chem. Solids* **1958**, *4*, 241.
(9) Moriya, T. New Mechanism of Anisotropic Superexchange Interaction. *Phys. Rev. Lett.* **1960**, *4*, 228−230.
(10) Moriya, T. Anisotropic Superexchange Interaction and Weak Ferromagnetism. *Phys. Rev.* **1960**, *120*, 91−98.
(11) Fert, A. R. Magnetic and Transport Properties of Metallic Multilayers. *MSF* **1991**, *59-60*, 439−480.
(12) Crépieux, A.; Lacroix, C. Dzyaloshinsky−Moriya interactions induced by symmetry breaking at a surface. *J. Magn. Magn. Mater.* **1998**, *182*, 341−349.
(13) Yang, H.; Thiaville, A.; Rohart, S.; Fert, A.; Chshiev, M. Anatomy of Dzyaloshinskii-Moriya Interaction at Co/Pt Interfaces. *Phys. Rev. Lett.* **2015**, *115*, 267210.
(14) Belabbes, A.; Bihlmayer, G.; Bechstedt, F.; Blügel, S.; Manchon, A. Hund's Rule-Driven Dzyaloshinskii-Moriya Interaction at 3*d*-5*d* Interfaces. *Phys. Rev. Lett.* **2016**, *117*, 247202.
(15) Lan, J.; Yu, W.; Wu, R.; Xiao, J. Spin-Wave Diode. *Phys. Rev. X* **2015**, *5*, 041049.
(16) Kim, J.-V.; Stamps, R. L.; Camley, R. E. Spin Wave Power Flow and Caustics in Ultrathin Ferromagnets with the Dzyaloshinskii-Moriya Interaction. *Phys. Rev. Lett.* **2016**, *117*, 197204.
(17) Brächer, T.; Boulle, O.; Gaudin, G.; Pirro, P. Creation of unidirectional spin-wave emitters by utilizing interfacial Dzyaloshinskii-Moriya interaction. *Phys. Rev. B* **2017**, *95*, 064429.
(18) Szulc, K.; Graczyk, P.; Mruczkiewicz, M.; Gubbiotti, G.; Krawczyk, M. Spin-Wave Diode and Circulator Based on Unidirectional Coupling. *Phys. Rev. Applied* **2020**, *14*, 034063.
(19) Chen, J.; Yu, H.; Gubbiotti, G. Unidirectional spin-wave propagation and devices. *J. Phys. D: Appl. Phys.* **2022**, *55*, 123001.
(20) Udvardi, L.; Szunyogh, L. Chiral Asymmetry of the Spin-Wave Spectra in Ultrathin Magnetic Films. *Phys. Rev. Lett.* **2009**, *102*, 207204.
(21) Cortés-Ortuño, D.; Landeros, P. Influence of the Dzyaloshinskii−Moriya interaction on the spin-wave spectra of thin films. *J. Phys: Cond. Matt.* **2013**, *25*, 156001.
(22) Moon, J.-H.; Seo, S.-M.; Lee, K.-J.; Kim, K.-W.; Ryu, J.; Lee, H.-W.; McMichael, R. D.; Stiles, M. D. Spin-wave propagation in the presence of interfacial Dzyaloshinskii-Moriya interaction. *Phys. Rev. B* **2013**, *88*, 184404.
(23) Di, K.; Zhang, V. L.; Lim, H. S.; Ng, S. C.; Kuok, M. H.; Yu, J.; Yoon, J.; Qiu, X.; Yang, H. Direct Observation of the Dzyaloshinskii-Moriya Interaction in a Pt/Co/Ni Film. *Phys. Rev. Lett.* **2015**, *114*, 047201.
(24) Nembach, H. T.; Shaw, J. M.; Weiler, M.; Jue, E.; Silva, T. J. Linear relation between Heisenberg exchange and interfacial Dzyaloshinskii-Moriya interaction in metal films. *Nat. Phys.* **2015**, *11*, 825−829.
(25) Tacchi, S.; Troncoso, R. E.; Ahlberg, M.; Gubbiotti, G.; Madami, M.; Åkerman, J.; Landeros, P. Interfacial Dzyaloshinskii-Moriya Interaction in Pt/CoFeB Films: Effect of the Heavy-Metal Thickness. *Phys. Rev. Lett.* **2017**, *118*, 147201.
(26) Lin, W.; Yang, B.; Chen, A. P.; Wu, X.; Guo, R.; Chen, S.; Liu, L.; Xie, Q.; Shu, X.; Hui, Y.; Chow, G. M.; Feng, Y.; Carlotti, G.; Tacchi, S.; Yang, H.; Chen, J. Perpendicular Magnetic Anisotropy and Dzyaloshinskii-Moriya Interaction at an Oxide/Ferromagnetic Metal Interface. *Phys. Rev. Lett.* **2020**, *124*, 217202.
(27) Ahmed, A. S.; Lee, A. J.; Bagués, N.; McCullian, B. A.; Thabt, A. M. A.; Perrine, A.; Wu, P.-K.; Rowland, J. R.; Randeria, M.; Hammel, P. C.; McComb, D. W.; Yang, F. Spin-Hall Topological Hall Effect in Highly Tunable Pt/Ferrimagnetic-Insulator Bilayers. *Nano Lett.* **2019**, *19*, 5683−5688.
(28) Wang, H.; et al. Chiral Spin-Wave Velocities Induced by All-Garnet Interfacial Dzyaloshinskii-Moriya Interaction in Ultrathin Yttrium Iron Garnet Films. *Phys. Rev. Lett.* **2020**, *124*, 027203.
(29) Schlitz, R.; Vélez, S.; Kamra, A.; Lambert, C.-H.; Lammel, M.; Goennenwein, S. T. B.; Gambardella, P. Control of Nonlocal Magnon Spin Transport via Magnon Drift Currents. *Phys. Rev. Lett.* **2021**, *126*, 257201.
(30) Fakhrul, T.; Huang, S.; Song, Y.; Khurana, B.; Beach, G. S. D.; Ross, C. A. Influence of substrate on interfacial Dzyaloshinskii-Moriya interaction in epitaxial $Tm_3Fe_5O_{12}$ films. *Phys. Rev. B* **2023**, *107*, 054421.
(31) Gallardo, R. A.; Cortés-Ortuño, D.; Troncoso, R. E.; Landeros, P. In *Three-Dimensional Magnonics: Layered, Micro- and Nanostructures*; Gubbiotti, G., Ed.; Jenny Stanford Publishing: 2019; pp 121−160.
(32) Kuepferling, M.; Casiraghi, A.; Soares, G.; Durin, G.; Garcia-Sanchez, F.; Chen, L.; Back, C. H.; Marrows, C. H.; Tacchi, S.; Carlotti, G. Measuring interfacial Dzyaloshinskii-Moriya interaction in ultrathin magnetic films. *Rev. Mod. Phys.* **2023**, *95*, 015003.
(33) Gladii, O.; Haidar, M.; Henry, Y.; Kostylev, M.; Bailleul, M. Frequency nonreciprocity of surface spin wave in permalloy thin films. *Phys. Rev. B* **2016**, *93*, 054430.
(34) Gallardo, R. A.; Alvarado-Seguel, P.; Schneider, T.; Gonzalez-Fuentes, C.; Roldán-Molina, A.; Lenz, K.; Lindner, J.; Landeros, P. Spin-wave non-reciprocity in magnetization-graded ferromagnetic films. *New J. Phys.* **2019**, *21*, 033026.
(35) Gallardo, R. A.; Schneider, T.; Chaurasiya, A. K.; Oelschlägel, A.; Arekapudi, S. S. P. K.; Roldán-Molina, A.; Hübner, R.; Lenz, K.; Barman, A.; Fassbender, J.; Lindner, J.; Hellwig, O.; Landeros, P. Reconfigurable Spin-Wave Nonreciprocity Induced by Dipolar Interaction in a Coupled Ferromagnetic Bilayer. *Phys. Rev. Applied* **2019**, *12*, 034012.
(36) Albisetti, E.; Tacchi, S.; Silvani, R.; Scaramuzzi, G.; Finizio, S.; Wintz, S.; Rinaldi, C.; Cantoni, M.; Raabe, J.; Carlotti, G.; Bertacco, R.; Riedo, E.; Petti, D. Optically Inspired Nanomagnonics with Nonreciprocal Spin Waves in Synthetic Antiferromagnets. *Adv. Mater.* **2020**, *32*, 1906439.
(37) Gallardo, R.; Alvarado-Seguel, P.; Landeros, P. Unidirectional Chiral Magnonics in Cylindrical Synthetic Antiferromagnets. *Phys. Rev. Appl.* **2022**, *18*, 054044.
(38) Otálora, J. A.; Yan, M.; Schultheiss, H.; Hertel, R.; Kákay, A. Curvature-Induced Asymmetric Spin-Wave Dispersion. *Phys. Rev. Lett.* **2016**, *117*, 227203.
(39) Landeros, P.; Otálora, J. A.; Streubel, R.; Kákay, A. In *Curvilinear Micromagnetism: From Fundamentals to Applications*; Makarov, D., Sheka, D. D., Eds.; Springer International: 2022; pp 163−213.
(40) Ma, F.; Zhou, Y. Interfacial Dzialoshinskii−Moriya interaction induced nonreciprocity of spin waves in magnonic waveguides. *RSC Adv.* **2014**, *4*, 46454−46459.
(41) Mruczkiewicz, M.; Krawczyk, M. Influence of the Dzyaloshinskii-Moriya interaction on the FMR spectrum of magnonic crystals and confined structures. *Phys. Rev. B* **2016**, *94*, 024434.
(42) Lee, S.-J.; Moon, J.-H.; Lee, H.-W.; Lee, K.-J. Spin-wave propagation in the presence of inhomogeneous Dzyaloshinskii-Moriya interactions. *Phys. Rev. B* **2017**, *96*, 184433.
(43) Gallardo, R. A.; Cortés-Ortuño, D.; Schneider, T.; Roldán-Molina, A.; Ma, F.; Troncoso, R. E.; Lenz, K.; Fangohr, H.; Lindner, J.; Landeros, P. Flat Bands, Indirect Gaps, and Unconventional Spin-Wave Behavior Induced by a Periodic Dzyaloshinskii-Moriya Interaction. *Phys. Rev. Lett.* **2019**, *122*, 067204.
(44) Zingsem, B. W.; Farle, M.; Stamps, R. L.; Camley, R. E. Unusual nature of confined modes in a chiral system: Directional transport in standing waves. *Phys. Rev. B* **2019**, *99*, 214429.
(45) Pan, H.; Zhang, V. L.; Di, K.; Kuok, M. H.; Lim, H. S.; Ng, S. C.; Singh, N.; Adeyeye, A. O. Phononic and magnonic dispersions of surface waves on a permalloy/BARC nanostructured array. *Nanoscale Res. Lett.* **2013**, *8*, 115.

https://doi.org/10.1021/acs.nanolett.2c04215
Nano Lett. 2023, 23, 6776−6783

(46) Mukherjee, S.; Spracklen, A.; Choudhury, D.; Goldman, N.; Öhberg, P.; Andersson, E.; Thomson, R. R. Observation of a Localized Flat-Band State in a Photonic Lieb Lattice. *Phys. Rev. Lett.* **2015**, *114*, 245504.
(47) Babu, N. K. P.; Trzaskowska, A.; Graczyk, P.; Centała, G.; Mieszczak, S.; Głowiński, H.; Zdunek, M.; Mielcarek, S.; Kłos, J. W. The Interaction between Surface Acoustic Waves and Spin Waves: The Role of Anisotropy and Spatial Profiles of the Modes. *Nano Lett.* **2021**, *21*, 946−951.
(48) Chen, J.; Zeng, L.; Wang, H.; Madami, M.; Gubbiotti, G.; Liu, S.; Zhang, J.; Wang, Z.; Jiang, W.; Zhang, Y.; Yu, D.; Ansermet, J.-P.; Yu, H. Magic-angle magnonic nanocavity in a magnetic moiré superlattice. *Phys. Rev. B* **2022**, *105*, 094445.
(49) Derzhko, O.; Richter, J.; Maksymenko, M. Strongly correlated flat-band systems: The route from Heisenberg spins to Hubbard electrons. *Int. J. Mod. Phys. B* **2015**, *29*, 1530007.
(50) Leykam, D.; Andreanov, A.; Flach, S. Artificial flat band systems: from lattice models to experiments. *Adv. Phys.: X* **2018**, *3*, 1473052.
(51) Suárez Morell, E.; Correa, J. D.; Vargas, P.; Pacheco, M.; Barticevic, Z. Flat bands in slightly twisted bilayer graphene: Tight-binding calculations. *Phys. Rev. B* **2010**, *82*, 121407.
(52) Cao, Y.; Fatemi, V.; Fang, S.; Watanabe, K.; Taniguchi, T.; Kaxiras, E.; Jarillo-Herrero, P. Unconventional superconductivity in magic-angle graphene superlattices. *Nature* **2018**, *556*, 43−50.
(53) Lu, X.; Stepanov, P.; Yang, W.; Xie, M.; Aamir, M. A.; Das, I.; Urgell, C.; Watanabe, K.; Taniguchi, T.; Zhang, G.; Bachtold, A.; MacDonald, A. H.; Efetov, D. K. Superconductors, orbital magnets and correlated states in magic-angle bilayer graphene. *Nature* **2019**, *574*, 653−657.
(54) Călugăru, D.; Chew, A.; Elcoro, L.; Xu, Y.; Regnault, N.; Song, Z.-D.; Bernevig, B. A. General construction and topological classification of crystalline flat bands. *Nat. Phys.* **2022**, *18*, 185−189.
(55) Kalesaki, E.; Delerue, C.; Morais Smith, C.; Beugeling, W.; Allan, G.; Vanmaekelbergh, D. Dirac Cones, Topological Edge States, and Nontrivial Flat Bands in Two-Dimensional Semiconductors with a Honeycomb Nanogeometry. *Phys. Rev. X* **2014**, *4*, 011010.
(56) Milićević, M.; Montambaux, G.; Ozawa, T.; Jamadi, O.; Real, B.; Sagnes, I.; Lemaître, A.; Le Gratiet, L.; Harouri, A.; Bloch, J.; Amo, A. Type-III and Tilted Dirac Cones Emerging from Flat Bands in Photonic Orbital Graphene. *Phys. Rev. X* **2019**, *9*, 031010.
(57) Lau, A.; Hyart, T.; Autieri, C.; Chen, A.; Pikulin, D. I. Designing Three-Dimensional Flat Bands in Nodal-Line Semimetals. *Phys. Rev. X* **2021**, *11*, 031017.
(58) Zhuo, L.; He, H.; Huang, R.; Li, Z.; Qiu, W.; Zhuang, F.; Su, S.; Lin, Z.; Huang, B.; Kan, Q. Flat band of Kagome lattice in graphene plasmonic crystals. *J. Phys. D: Appl. Phys.* **2022**, *55*, 065106.
(59) Gubbiotti, G.; Tacchi, S.; Carlotti, G.; Vavassori, P.; Singh, N.; Goolaup, S.; Adeyeye, A. O.; Stashkevich, A.; Kostylev, M. Magnetostatic interaction in arrays of nanometric permalloy wires: A magneto-optic Kerr effect and a Brillouin light scattering study. *Phys. Rev. B* **2005**, *72*, 224413.
(60) Zhang, V. L.; Ma, F. S.; Pan, H. H.; Lin, C. S.; Lim, H. S.; Ng, S. C.; Kuok, M. H.; Jain, S.; Adeyeye, A. O. Observation of dual magnonic and phononic bandgaps in bi-component nanostructured crystals. *Appl. Phys. Lett.* **2012**, *100*, 163118.
(61) Di, K.; Zhang, V. L.; Kuok, M. H.; Lim, H. S.; Ng, S. C.; Narayanapillai, K.; Yang, H. Band structure of magnonic crystals with defects: Brillouin spectroscopy and micromagnetic simulations. *Phys. Rev. B* **2014**, *90*, 060405.
(62) Gallardo, R. A.; Schneider, T.; Roldán-Molina, A.; Langer, M.; Fassbender, J.; Lenz, K.; Lindner, J.; Landeros, P. Dipolar interaction induced band gaps and flat modes in surface-modulated magnonic crystals. *Phys. Rev. B* **2018**, *97*, 144405.
(63) Gallardo, R. A.; Schneider, T.; Roldán-Molina, A.; Langer, M.; Núñez, A. S.; Lenz, K.; Lindner, J.; Landeros, P. Symmetry and localization properties of defect modes in magnonic superlattices. *Phys. Rev. B* **2018**, *97*, 174404.
(64) Tacchi, S.; Gubbiotti, G.; Madami, M.; Carlotti, G. Brillouin light scattering studies of 2D magnonic crystals. *J. Phys.: Condens. Matter* **2017**, *29*, 073001.
(65) Zeng, C.; Elser, V. Numerical studies of antiferromagnetism on a Kagomé net. *Phys. Rev. B* **1990**, *42*, 8436−8444.
(66) Matan, K.; Grohol, D.; Nocera, D. G.; Yildirim, T.; Harris, A. B.; Lee, S. H.; Nagler, S. E.; Lee, Y. S. Spin Waves in the Frustrated Kagomé Lattice Antiferromagnet $KFe_3(OH)_6(SO_4)_2$. *Phys. Rev. Lett.* **2006**, *96*, 247201.
(67) Chisnell, R.; Helton, J. S.; Freedman, D. E.; Singh, D. K.; Bewley, R. I.; Nocera, D. G.; Lee, Y. S. Topological Magnon Bands in a Kagome Lattice Ferromagnet. *Phys. Rev. Lett.* **2015**, *115*, 147201.
(68) Pershoguba, S. S.; Banerjee, S.; Lashley, J. C.; Park, J.; Ågren, H.; Aeppli, G.; Balatsky, A. V. Dirac Magnons in Honeycomb Ferromagnets. *Phys. Rev. X* **2018**, *8*, 011010.
(69) Mook, A.; Plekhanov, K.; Klinovaja, J.; Loss, D. Interaction-Stabilized Topological Magnon Insulator in Ferromagnets. *Phys. Rev. X* **2021**, *11*, 021061.
(70) Stashkevich, A. A.; Belmeguenai, M.; Roussigné, Y.; Cherif, S. M.; Kostylev, M.; Gabor, M.; Lacour, D.; Tiusan, C.; Hehn, M. Experimental study of spin-wave dispersion in Py/Pt film structures in the presence of an interface Dzyaloshinskii-Moriya interaction. *Phys. Rev. B* **2015**, *91*, 214409.
(71) Landeros, P.; Mills, D. L. Spin waves in periodically perturbed films. *Phys. Rev. B* **2012**, *85*, 054424.
(72) Gallardo, R. A.; Banholzer, A.; Wagner, K.; Körner, M.; Lenz, K.; Farle, M.; Lindner, J.; Fassbender, J.; Landeros, P. Splitting of spin-wave modes in thin films with arrays of periodic perturbations: theory and experiment. *New J. Phys.* **2014**, *16*, 023015.
(73) Barsukov, I.; Landeros, P.; Meckenstock, R.; Lindner, J.; Spoddig, D.; Li, Z.-A.; Krumme, B.; Wende, H.; Mills, D. L.; Farle, M. Tuning magnetic relaxation by oblique deposition. *Phys. Rev. B* **2012**, *85*, 014420.
(74) Körner, M.; Lenz, K.; Gallardo, R. A.; Fritzsche, M.; Mücklich, A.; Facsko, S.; Lindner, J.; Landeros, P.; Fassbender, J. Two-magnon scattering in permalloy thin films due to rippled substrates. *Phys. Rev. B* **2013**, *88*, 054405.
(75) Belmeguenai, M.; Bouloussa, H.; Roussigné, Y.; Gabor, M. S.; Petrisor, T.; Tiusan, C.; Yang, H.; Stashkevich, A.; Chérif, S. M. Interface Dzyaloshinskii-Moriya interaction in the interlayer antiferromagnetic-exchange coupled Pt/CoFeB/Ru/CoFeB systems. *Phys. Rev. B* **2017**, *96*, 144402.
(76) Natarajarathinam, A.; Tadisina, Z. R.; Mewes, T.; Watts, S.; Chen, E.; Gupta, S. Influence of capping layers on CoFeB anisotropy and damping. *J. Appl. Phys.* **2012**, *112*, 053909.
(77) Liu, Y.; Zhang, J.; Wang, S.; Jiang, S.; Liu, Q.; Li, X.; Wu, Z.; Yu, G. Ru Catalyst-Induced Perpendicular Magnetic Anisotropy in MgO/CoFeB/Ta/MgO Multilayered Films. *ACS Appl. Mater. & Interfaces* **2015**, *7*, 26643−26648.
(78) Gnani, E.; Reggiani, S.; Rudan, M. Density of states and group velocity of electrons in SiO_2 calculated from a full band structure. *Phys. Rev. B* **2002**, *66*, 195205.
(79) Camley, R. E.; Grünberg, P.; Mayr, C. M. Stokes—anti-Stokes asymmetry in Brillouin scattering from magnons in thin ferromagnetic films. *Phys. Rev. B* **1982**, *26*, 2609−2614.
(80) Cochran, J. F.; From, M.; Heinrich, B. Dependence of anti-Stokes/Stokes intensity ratios on substrate optical properties for Brillouin light scattering from ultrathin iron films. *J. Appl. Phys.* **1998**, *83*, 6296−6298.
(81) Gao, Y.; Tian, Y.; Zhang, Y.; Chai, G. Study of the intensity asymmetry in Brillouin light scattering from magnons in FeNi thin films. *J. Magn. Magn. Mater.* **2020**, *504*, 166671.
(82) See the Supporting Information.

https://doi.org/10.1021/acs.nanolett.2c04215
Nano Lett. 2023, 23, 6776−6783